Generation and time jitter of the loose soliton bunch in a passively mode-locked fiber laser

Zhenhong Wang (王振洪), Zhi Wang (王 志)*, Yan'ge Liu (刘艳格), Ruijing He (贺瑞敬), Guangdou Wang (王光斗), Guang Yang (杨 光), and Simeng Han (韩思濛)

Key Laboratory of Optical Information and Technology, Ministry of Education, Tianjin Key Laboratory of Optoelectronic Sensor and Sensing Network Technology, and Institute of Modern Optics, Nankai University, Tianjin 300350, China

**Corresponding author: zhiwang@nankai.edu.cn*

Received March 10, 2017; accepted May 18, 2017; posted online June 7, 2017

We report a regime of the loose soliton bunch in an erbium-doped passively mode-locked fiber laser. In this state, every soliton bunch consists of multiple pulses. The amount of multiple pulses inside the soliton bunch increase as the pump power rises. Moreover, the temporal average pulse-to-pulse separation decreases in general with the increase of the pump power. Further, the spatial-temporal sequences based on the dispersive Fourier transformation technique show that pulse-to-pulse interactions and time jitter can result in pulse forking inside the soliton bunch. Finally, we theoretically demonstrate the soliton bunch with different pulse-to-pulse separations.

OCIS codes: 060.5530, 140.4050, 140.3500, 320.7120.
doi: 10.3788/COL201715.080605.

Passively mode-locked fiber lasers (PMLFLs) could be not only used as simple and economic ultrashort pulse sources but also as an ideal platform for exploring the nonlinear dynamics of dissipative solitons[1,2] such as bound solitons[3–9], soliton rains[10,11], noise-like pulses[12,13], sideband-controllable solitons[14], soliton resonance[15], and soliton explosions[16,17]. Due to energy quantization, multiple solitons are apt to be generated in the net anomalous dispersion PMLFLs when increasing pump power to a certain value[18]. Owing to the variety of interaction mechanisms, these multiple solitons will always interact and thus form different kinds of operation states. For example, the interactions based on the acousto-optic effect are both attractive and repulsive at long range and thus promote a regular distribution of the soliton pulses in the laser cavity, namely harmonic mode locking (HML)[19]. The interactions based on coherent pulse overlap, slow recovery, and depletion processes of the gain or/and dispersive wave, which can lock both the relative timing and phase of neighboring pulses, lead to soliton pairs[20,21] or multiple-soliton bound states[22]. According to the pulse-to-pulse separation, the bound state can be distributed into two types: tightly or loosely bound state[7]. The tightly bound solitons have special soliton separations, which exhibit fixed discrete values, and a fixed 0, $\pi/2$, or π phase difference[4,23–25]. In contrast, the loosely bound solitons usually have unfixed discrete soliton pulse separations and unfixed soliton phase differences[7]. Due to relatively weak interactions, the loosely bound solitons are intrinsically unstable, which could induce comparatively complex spatiotemporal processes. However, limited by the resolution of the photodetection, this timing instability in the shot-to-shot scale has rarely been observed experimentally.

Recently, there has been a substantial advance in real-time high speed oscilloscopes that can make it possible to conduct real-time spatial-temporal intensity dynamics measurements. The real-time dynamics measuring method based on the dispersive Fourier transformation (DFT) technique has been used for the study of noise-like pulses[12], unstable soliton bunches[26], and rogue waves[27,28] in MLFLs. In this Letter, we observe the shot-to-shot time jitter in loose soliton bunches by the DFT technique. The soliton bunches, consisting of multiple pulses with intervals of tens of picoseconds, are generated in a PMLFL with a graphene saturable absorber (GSA). The evolution of the spatial-temporal dynamics is recorded by a high-speed real-time oscilloscope and the DFT technique. The time jitter is investigated by the forking and merging of the interference fringes in the spatial-temporal diagram based on the DFT technique.

The experimental setup is shown in Fig. 1. The gain medium is a piece of 1 m long erbium-doped fiber (EDF, LIEKKI Er80-8/125) with a dispersion parameter of 15.7 ps/(nm · km) that is pumped by a 980 nm laser diode (LD) through a fused wavelength division multiplexer (WDM). The other fibers are about a 14.5 m standard single-mode fiber (SMF) with a dispersion parameter of 18 ps/(nm · km). So, the net cavity dispersion is negative. A polarization independent isolator (PI-ISO) and a polarization controller (PC) are used to maintain the unidirectional laser pulse propagation and adjust the polarization states in the cavity, respectively. The laser output is directed through the 10% port of an optical coupler (OC). The fiber laser is mode locked by a GSA on microfiber, which is prepared by the covering method[29]. The total cavity length is about 15.5 m. The laser output is monitored by an optical spectrum analyzer (YOKOGAVA AQ6370C), an oscilloscope (LeCroy WaveRunner 620Zi) with a 5 GHz bandwidth photodetector (DET08CFC), and an autocorrelator (FR-103XL). The

 © 2017 Chinese Optics Letters

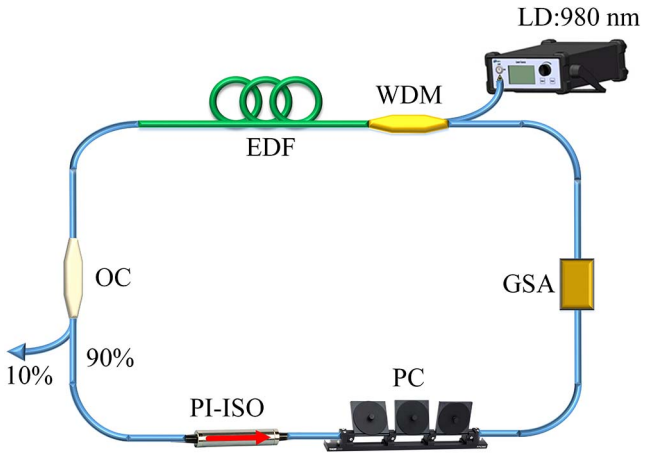

Fig. 1. Schematic setup of the fiber ring laser cavity.

real-time spatial-temporal intensity dynamics are evaluated by a 50 GHz bandwidth photodetector (U2T XPDV2120R) and a 36 GHz real-time oscilloscope with a maximal sampling rate of 80 GS/s (LeCroy LCRY3312N69578).

By adjusting the PC, the stable single-pulse soliton mode locking can be obtained at a pump power of 70 mW. When the pump power is increased to 160 mW, multiple solitons can be observed through properly rotating the paddles of the PC. The optical spectra under different pump powers are shown in Fig. 2(a) with other conditions unchanged. Figure 2(b) is the close-up of the dotted part in Fig. 2(a). Obviously, the spectra of multiple solitons are strongly modulated and have a high interference pattern. The spectral period in Fig. 2(b) is about 0.23 nm, which corresponds to a temporal separation of 35 ps. The output pulse trains at different pump powers are almost the same, as shown in the inset of Fig. 2(b), where we can calculate that the pulse repetition rate is the fundamental one of 12.9 MHz.

In order to further investigate the details of the soliton bunch, we conduct the spatial-temporal measures by employing a high-speed oscilloscope (36 GHz and 80 GS/s). The corresponding measuring results, in which the three-dimensional spatial-temporal intensity evolutions of the soliton bunch are displayed over 10000 consecutive round trips, are shown in Figs. 3(a) and 3(b). Clearly, there is a constant pulse amount when the pump power is fixed and the amount of pulses increases as the pump power increases. In fact, the amount changes from 6 to 29 when the pump power increases from 160 to 520 mW. In addition, the temporal pulse-to-pulse separations are variational in the range of tens of picoseconds at the same pump power. As shown in Fig. 3(a), the pulse-to-pulse separation inside the six-soliton alters from 55 to 51 ps, later to 51 ps, then to 56 ps, and last to 61 ps. However, the whole last variation trend is incremental. We calculate the average pulse-to-pulse separations at different pump powers, shown in Fig. 3(c). Obviously, the general tendency is declining. The pulse-to-pulse separation is about

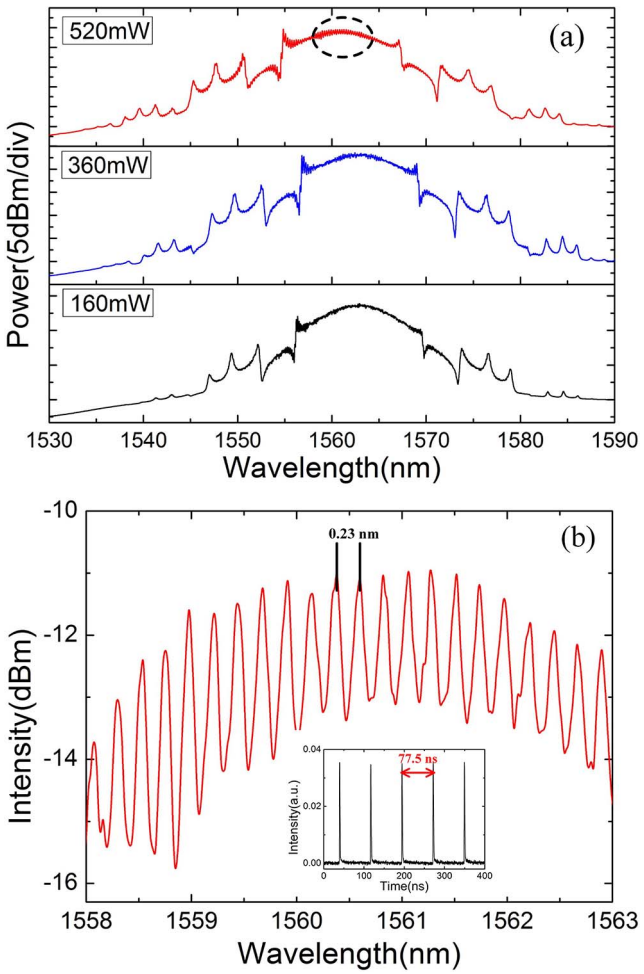

Fig. 2. (a) The spectra at different pump power and (b) the close-up of the dotted part in (a). Inset: The output pulse train.

34 ps at the pump power of 520 mW, corresponding to the spectral period of 0.238 nm, which is generally consistent with the spectral period in Fig. 2(b). Both the slow recovery and depletion processes of the gain in the cavity play a vital role in the formation of the multiple pulses and variational pulse-to-pulse separations[30].

Further, we make spatial-temporal measures based on the DFT technique. A length of 25 km SMF is used to stretch output pulses. Therefore, the spectral resolution of our measurements is approximately 0.024 THz (0.2 nm)[31]. The spatial-temporal sequences of the soliton bunch at the pump powers of 160 and 360 mW are shown in Fig. 4. Figures 4(c) and 4(d) are the close-ups of Figs. 4(a) and 4(b), respectively. Obviously, Fig. 4 can clearly show that there is a strong interaction and a strong time jitter among multiple pulses at consecutive round trips. Section A in Fig. 4(c) indicates that the multiple pulses start to fork at the influence of the strong interaction. Then, section B in Fig. 4(c) indicates that the multiple pulses begin to merge together. Subsequently, section C in Fig. 4(c) shows that these pulses are set to fork again. Finally, section D in Fig. 4(c) shows that the pulses start to merge together. Here, we should note

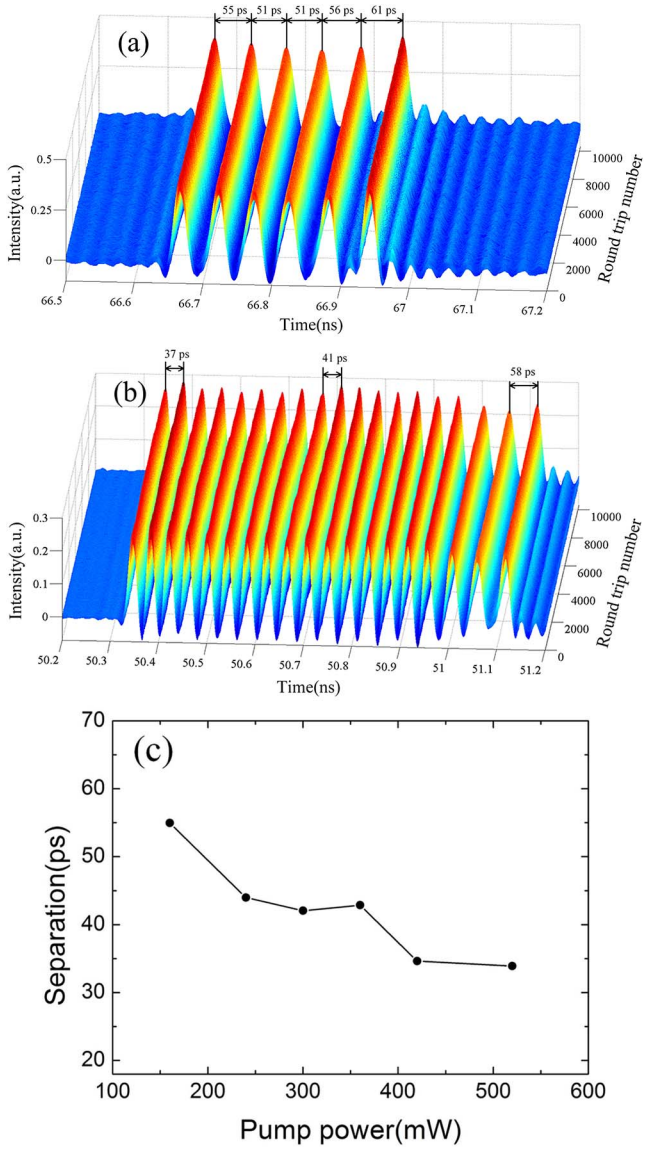

Fig. 3. (a) The spatial-temporal diagram for a pump power of 160 mW. (b) The spatial-temporal diagram for a pump power of 360 mW. (c) The average pulse interval in the soliton bunch at the different pump powers.

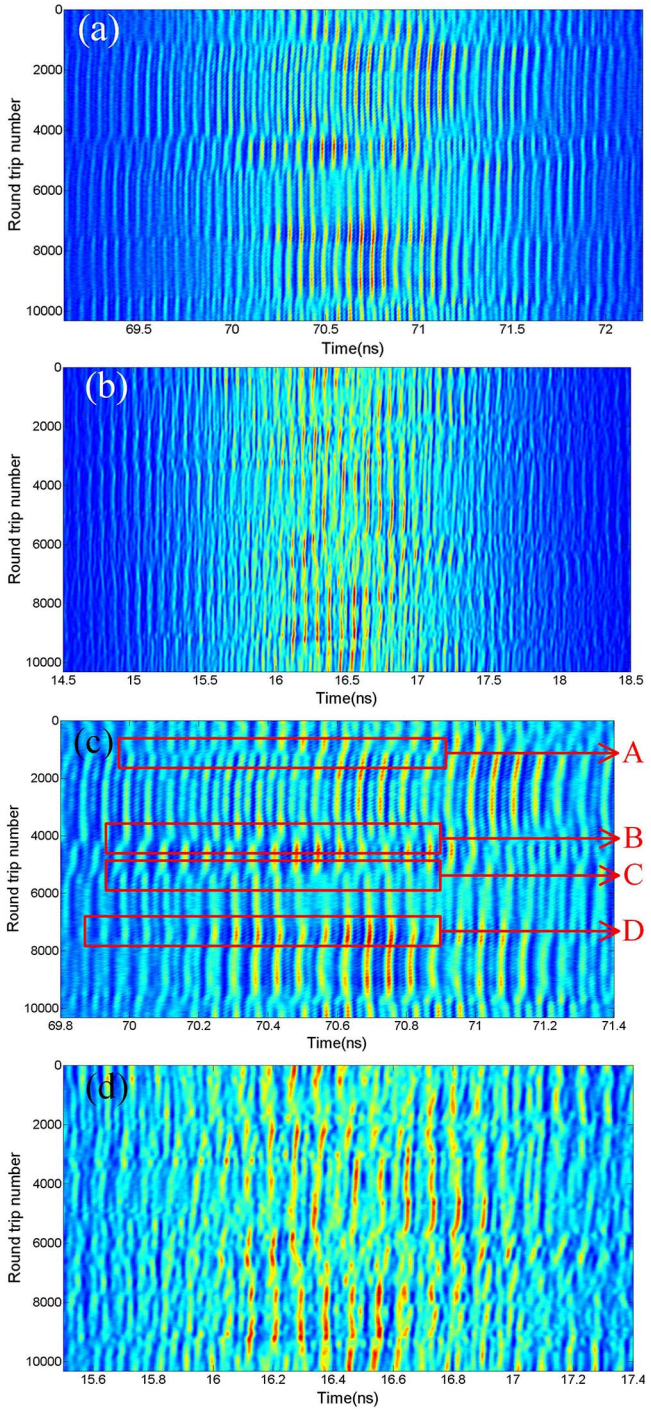

Fig. 4. (a) The spatial-temporal diagram for a pump power of 160 mW. (b) The spatial-temporal diagram for a pump power of 360 mW. (c) and (d) are the close-ups of (a) and (b), respectively.

that the DFT may difficultly map the shot-shot optical spectrum of the optical pulse on account of the strong multiple-pulse interaction. Therefore, we cannot get the averaged DFT spectrum.

In order to further understand the interference patterns in the spatial-temporal diagram, we give a simple discussion about the DFT technique for a soliton bunch. Assume that the complex amplitude of the slowly varying envelope of a soliton bunch can be described by the superposition of solitons, which is given by

$$U_0(T) = \sum_{k=1}^{N} u_k(T - \tau_k) e^{-i\phi_k}, \tag{1}$$

where N is the number of solitons, u_k, τ_k, and ϕ_k are the slowly varying envelope, relative position, and relative phase of a single soliton, respectively. Then the output intensity profile after the dispersive fiber is proportional to the spectral interference of the solitons in a bunch[31],

$$|U_L(T)|^2 \propto \left| \sum_{k=1}^{N} \tilde{u}_k \left(\frac{T - \tau_k}{\beta_2 L} \right) e^{-i\phi_k} \right|^2, \tag{2}$$

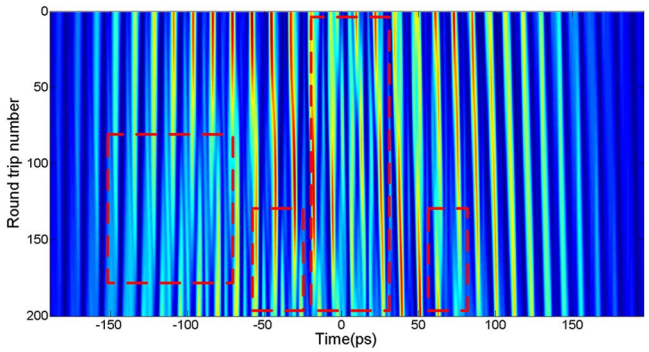

Fig. 5. Spatial-temporal diagram at the six-soliton state.

where $\tilde{u}_k$ denotes the Fourier transform of an input single soliton, β_2 is the second-order dispersion coefficient, and L is length of the dispersive fiber. Equation (2) indicates that the fringe patterns in the spatial-temporal diagram are sensitive to the time jitter of the relative position and phase of each soliton. For example, we assume that the soliton pitches in Fig. 3(a) are varied by 2, 2, 1, 2, and 3 ps in 200 round trips, respectively, and numerically simulate the spatial-temporal diagram outputted from 25 km SMF (shown in Fig. 5). Clearly, we can observe the obvious interference pattern and multiple-pulse forking in the sections of the dotted lines, which is related to the time jitter in PMLFL. These characters generally agree with the phenomenon in Fig. 4. Although only six solitons were considered, the obtained pulse-to-pulse forking in the regime can be well pronounced.

In conclusion, we observe the loose soliton bunch operation in an erbium-doped PMLFL. The influence of slow recovery and depletion in the laser takes most responsibility in the formation of the multiple pulses and variational separations of pulses in the loose soliton bunch. In the regime, the single-soliton bunch consists of multiple pulses and the amount of pulses in each soliton bunch increases when the pump power rises. In addition, the pulse-to-pulse separation is on the whole increasing over a range of tens of picoseconds and the average pulse separation is decreasing in general with the increase of the pump power. Furthermore, the spatial-temporal sequences based on the DFT technique show that multiple pulse forking exists inside the soliton bunch, which can indicate that the interaction and the time jitter of multiple pulses inside the soliton bunch are strong. Finally, we numerically analyze the multiple-pulse interactions and the time jitter at different pulse-to-pulse separations. We hope that these results can further help to understand the dynamics of multiple pulses in the soliton bunch.

This work was supported by the National Natural Science Foundation of China (NSFC) (Nos. 11674177, 61322510, and 61640408) and the Tianjin Natural Science Foundation (Nos. 16JCZDJC31000 and 14JCZDJC31300).

References

1. M. E. Fermann and I. Hartl, Nat. Photonics **7**, 868 (2013).
2. C. Xu and F. Wise, Nat. Photonics **7**, 875 (2013).
3. Y. Gong, P. Shum, T. Hiang, Q. Wen, and D. Tang, Opt. Commun. **200**, 389 (2001).
4. D. Tang, W. Man, H. Tam, and P. Drummond, Phys. Rev. A **64**, 033814 (2001).
5. N. Seong and D. Y. Kim, Opt. Lett. **27**, 1321 (2002).
6. D. Tang, B. Zhao, D. Shen, C. Lu, W. Man, and H. Tam, Phys. Rev. A **66**, 033806 (2002).
7. X. Wu, D. Tang, X. Luan, and Q. Zhang, Opt. Commun. **284**, 3615 (2011).
8. L. Gui, X. Xiao, and C. Yang, J. Opt. Soc. Am. B **30**, 158 (2013).
9. L. Zhao, D. Tang, and D. Liu, Appl. Phys. B. **99**, 441 (2010).
10. S. Chouli and P. Grelu, Opt. Express **17**, 11776 (2009).
11. S. Chouli and P. Grelu, Phys. Rev. A **81**, 063829 (2010).
12. A. F. Runge, C. Aguergaray, N. G. Broderick, and M. Erkintalo, Opt. Lett. **38**, 4327 (2013).
13. S. Liu, F. Yan, Y. Li, L. Zhang, Z. Bai, H. Zhou, and Y. Hou, Photon. Res. **4**, 318 (2016).
14. S. Tan, Z. Tiu, S. Harun, and H. Ahmad, Chin. Opt. Lett. **13**, 111406 (2015).
15. Z. Wang, S. Du, J. Wang, F. Zou, Z. Wang, W. Wu, and J. Zhou, Chin. Opt. Lett. **14**, 041401 (2016).
16. A. F. Runge, N. G. Broderick, and M. Erkintalo, Optica **2**, 36 (2015).
17. M. Liu, A.-P. Luo, Y.-R. Yan, S. Hu, Y.-C. Liu, H. Cui, Z.-C. Luo, and W.-C. Xu, Opt. Lett. **41**, 1181 (2016).
18. D. Tang, L. Zhao, B. Zhao, and A. Liu, Phys. Rev. A **72**, 043816 (2005).
19. A. Grudinin and S. Gray, J. Opt. Soc. Am. B **14**, 144 (1997).
20. N. Akhmediev, A. Ankiewicz, and J. Soto-Crespo, J. Opt. Soc. Am. B **15**, 515 (1998).
21. P. Grelu, F. Belhache, F. Gutty, and J.-M. Soto-Crespo, Opt. Lett. **27**, 966 (2002).
22. N. Akhmediev, A. Ankiewicz, and J. Soto-Crespo, Phys. Rev. Lett. **79**, 4047 (1997).
23. B. A. Malomed, Phys. Rev. A **44**, 6954 (1991).
24. B. A. Malomed, Phys. Rev. E **47**, 2874 (1993).
25. P. Grelu, J. Béal, and J. Soto-Crespo, Opt. Express **11**, 2238 (2003).
26. Z. Wang, Z. Wang, Y.-g. Liu, W. Zhao, H. Zhang, S. Wang, G. Yang, and R. He, Opt. Express **24**, 14709 (2016).
27. Z.-R. Cai, M. Liu, S. Hu, J. Yao, A.-P. Luo, Z.-C. Luo, and W.-C. Xu, IEEE J. Sel. Top. Quantum Electron. **53**, 1 (2017).
28. C. Lecaplain and P. Grelu, Phys. Rev. A **90**, 013805 (2014).
29. Q. Sheng, M. Feng, W. Xin, T. Han, Y. Liu, Z. Liu, and J. Tian, Opt. Express **21**, 14859 (2013).
30. A. Zaviyalov, P. Grelu, and F. Lederer, Opt. Lett. **37**, 175 (2012).
31. K. Goda and B. Jalali, Nat. Photonics **7**, 102 (2013).